

# Physics of the Solid State

<p><b>COUNTRY</b></p> <p>United States</p> <p>Universities and research institutions in United States</p> <p>Media Ranking in United States</p>	<p><b>SUBJECT AREA AND CATEGORY</b></p> <p>Materials Science</p> <ul style="list-style-type: none"> <li>Electronic, Optical and Magnetic Materials</li> </ul> <p>Physics and Astronomy</p> <ul style="list-style-type: none"> <li>Condensed Matter Physics</li> </ul>	<p><b>PUBLISHER</b></p> <p>Pleiades Publishing</p>
<p><b>H-INDEX</b></p> <p><b>52</b></p>	<p><b>PUBLICATION TYPE</b></p> <p>Journals</p>	<p><b>ISSN</b></p> <p>10637834, 10906460</p>
<p><b>COVERAGE</b></p> <p>1996-2021</p>	<p><b>INFORMATION</b></p> <p><a href="#">Homepage</a></p> <p><a href="#">How to publish in this journal</a></p> <p><a href="mailto:sst@journals.ioffe.rssi.ru">sst@journals.ioffe.rssi.ru</a></p>	

**SCOPE**

Presents the latest results from Russia's leading researchers in condensed matter physics at the Russian Academy of Sciences and other prestigious institutions. Covers all areas of solid state physics including solid state optics, solid state acoustics, electronic and vibrational spectra, phase transitions, ferroelectricity, magnetism, and superconductivity. Also presents review papers on the most important problems in solid state physics.

**Physics of the Solid State**

Q3

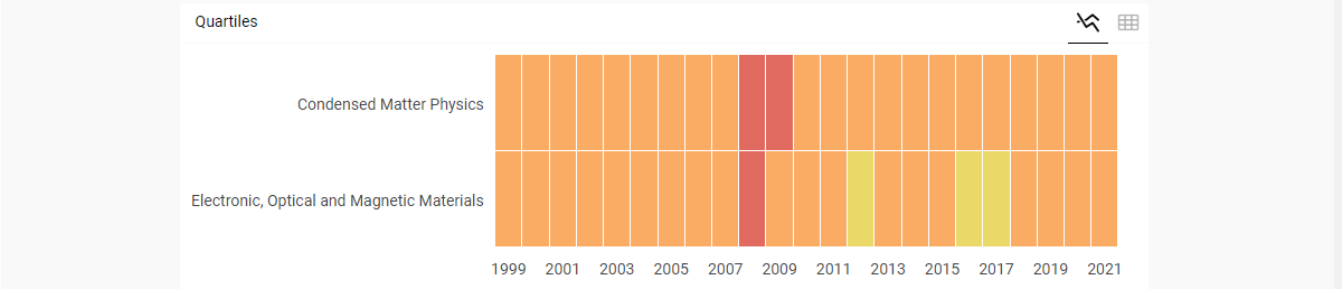
Condensed Matter Physics

best quartile

**SJR 2021**

0.28

powered by scimagojr.com



# Molecular Dynamics Study of the Effect of Carbon and Oxygen Impurities on the Velocity of the Crystallization Front in Nickel

G. M. Poletaev<sup>a,\*</sup>, R. Y. Rakitin<sup>b</sup>, and V. V. Kovalenko<sup>c</sup>

<sup>a</sup> Polzunov Altai State Technical University, Barnaul, Russia

<sup>b</sup> Altai State University, Barnaul, Russia

<sup>c</sup> Siberian State Industrial University, Novokuznetsk, Russia

\*e-mail: gmpoletaev@mail.ru

Received August 12, 2022; revised August 19, 2022; accepted August 24, 2022

**Abstract**—The effect of carbon and oxygen impurities on the velocity of the crystallization front in nickel is studied using molecular dynamics simulation. Three different orientations of the front relative to the growing crystal were considered: (100), (110), and (111). Impurity atoms were introduced randomly over the entire volume of the computational cell. The impurity concentration varied from 0 to 7 at %. It was found that the introduction of impurity atoms in all cases significantly reduces the crystallization velocity, wherein oxygen atoms slow down the crystallization front more strongly than carbon atoms. The mechanism of deceleration of crystallization by impurity atoms is associated with two factors: deceleration of self-diffusion in a liquid metal due to the formation of relatively strong bonds between metal atoms and impurity atoms (for oxygen, this bond is stronger than that for carbon atoms), and distortion of the crystal lattice due to the dilatation effect around impurity atoms in a growing crystal (this effect is also higher for oxygen atoms). In the case of carbon impurity at sufficiently high concentrations (on the order of several percent), carbon atoms form aggregates, which are accumulations of several tens of carbon atoms in the metal matrix. The crystallization front lingered on these aggregates. During crystallization in the presence of oxygen impurities, aggregates are not observed. The orientation of the crystallization front influences the crystallization velocity: crystallization proceeds faster with the (100) orientation, and slower with the (111) orientation. This anisotropy of the velocity of the crystallization front is due to the difference in the free energies of the metal atom in the liquid phase and that “embedded” into the boundary of the growing crystal.

**Keywords:** molecular dynamics, metal, crystallization, carbon, oxygen

**DOI:** 10.1134/S1063783422090062

## 1. INTRODUCTION

Crystallization of metals and alloy plays an important part in technological operations, and its progress determines many properties of materials. However, in spite of the interest to this problem and a long history of its studying, the problems regarding the kinetics and features of the homogeneous crystallization mechanism [1–3] related to the nucleation of crystallization nuclei and comparatively simpler heterogeneous mechanisms [4–8], when considering the crystal–melt front motion, remain unsolved up to now.

By now, as a result of appearance of the deep overcooling technology and computer simulation [7], it became known that the crystallization front motion velocity increases not always as temperature decreases, i.e., the overcooling increases, but only to a temperature of  $0.6–0.8T_m$ , and then it even starts to decrease. Similar behavior is better described by so called kinetic diffusion limited model, which was considered for a

long time along with the competing collision limited model [1, 4, 7]. In addition, recently, mainly owing to computer simulation [5, 9–12], it was revealed that the crystallization front velocity is dependent on the orientation with respect to a growing crystal. It is shown that, in the case of fcc crystals, the crystallization front velocity is highest at the orientation along the (100) plane.

In our previous work [13] devoted to the simulation of the crystallization of nickel and silver in the presence of carbon and oxygen impurities, it was revealed that these impurities of light elements lead to substantial slowing-down of the crystallization. It was concluded that the slowing-down of the crystallization front by the impurity atoms is related to the local crystal lattice deformation caused by the impurities and, as a rule, the larger this deformation, the stronger impurity atoms decelerate the crystallization front.

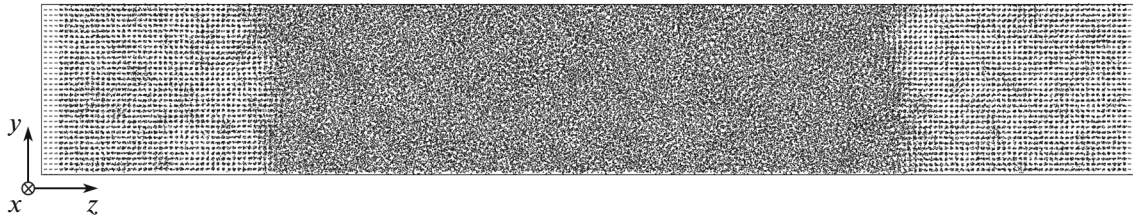


Fig. 1. Calculation cell with orientation  $XY$  (100) after the simulation of the crystallization at 1500 K for 75 ps.

This work is a continuation of those studies, but only using nickel as an example. Unlike [13], where comparatively small models including about 20000 atoms with the only orientation of the crystallization front along plane (111) were considered, in this work, we use the models including much more atoms (about 110000) and consider various versions of the crystallization front orientation: (100), (111), and (110).

### MODEL

The computational cell in the molecular-dynamic model was a long parallelepiped with a square cross-section (Fig. 1). At the lateral faces, i.e., along axes  $X$  and  $Y$ , periodic boundary conditions were used. To imitate the initial position of the crystallization front at the ends along axis  $Z$  (at the ends on the left and on the right in Fig. 1), the crystal structure was fixed: atoms shown by a light-grey color in Fig. 1 remain immobile during the simulation. We considered three calculation cells with various orientations of the  $XY$  plane, i.e., the crystallization front: (100), (110), and (111). The computational cells contained more 110000 atoms, not including impurity atoms, and had the widths and the heights of  $\sim 5.8$  nm and the length, about 37.5 nm.

The interactions of nickel atoms to each other were described in this model using the Cleri–Rosato multiparticle potential [14] created using the tight-binding model. The interactions of carbon and oxygen atoms with nickel atoms and to each other were calculated using the Morse potentials developed in [15]. These potentials were successfully used when solving various problems, and they describe various properties of nickel and carbon and oxygen impurities quite well [15–20].

Before main computer experiments, the created computational cells were melting by giving a temperature significantly higher than the melting temperature and exposure for a time that is sufficient to completely melt the cell structure. The fracture of the crystal structure and its melting were registered quite simply not only visually, but also by the radial distribution (pair correlation) diagrams. After the melted computational cells with three various orientations of the crystal structure fixed on the left and on the right ends

were obtained, impurity carbon or oxygen atoms were introduced. The impurity atoms were added randomly over entire cell volume. The impurity atom concentration was varied from 0 to 7 at %.

The crystallization was simulated, maintaining a constant temperature using a Nose–Hoover thermostat. The main results were obtained for temperatures 1500 and 1200 K. When given one or other temperatures, the computational cell sizes were changes taking into account the thermal expansion coefficient. But the cell volume remains constant during simulation of crystallization at a constant temperature. The repeated counting time step was varied, but it was 5 fs in most cases.

### RESULTS AND DISCUSSION

As may be seen from Fig. 1, the crystallization front moved, during the computer experiment, from the left and the right ends to the computational cell center. In most cases, the front position was well observed visually (in particular, after the abrupt cooling, during which the amorphous part had not time to crystallize, but the crystalline planes were seen more clearly). In [8], it was shown that the crystallization front moves a large part of its way at almost the same velocity. Thus its velocity was calculated as the ratio of the displacements of the crystallization front from the left and the right ends to the simulation time. Figure 2 shows the dependences of the crystallization front velocity on the impurity carbon and oxygen atom concentrations for the three front orientations at 1500 K ( $0.87T_m$ ); Fig. 3 shows these dependences at 1200 K ( $0.70T_m$ ). It should be noted that the maximum crystallization velocity obtained in this work coincides with the values obtained in [9] for nickel by computer simulation with another potential: 150 m/s for orientation (100) and 100 m/s for orientation (110).

As is seen for Figs. 2 and 3, the introduction of impurity atoms in all the cases substantially decreased the crystallization velocity. According to the obtained data, oxygen atoms decelerate the crystallization front more substantially than carbon atoms do. All the obtained dependences show that the character of the influence of the impurities is almost the same.

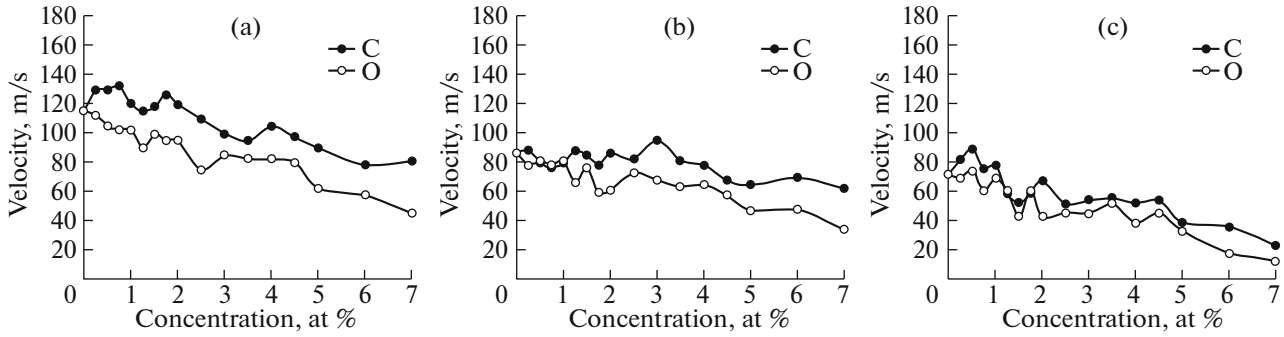


**Fig. 2.** Crystallization front motion velocity vs. the concentration of impurity carbon and oxygen atoms at the thermostat temperature 1500 K at the front orientation along planes (a) (100), (b) (110), and (c) (111).

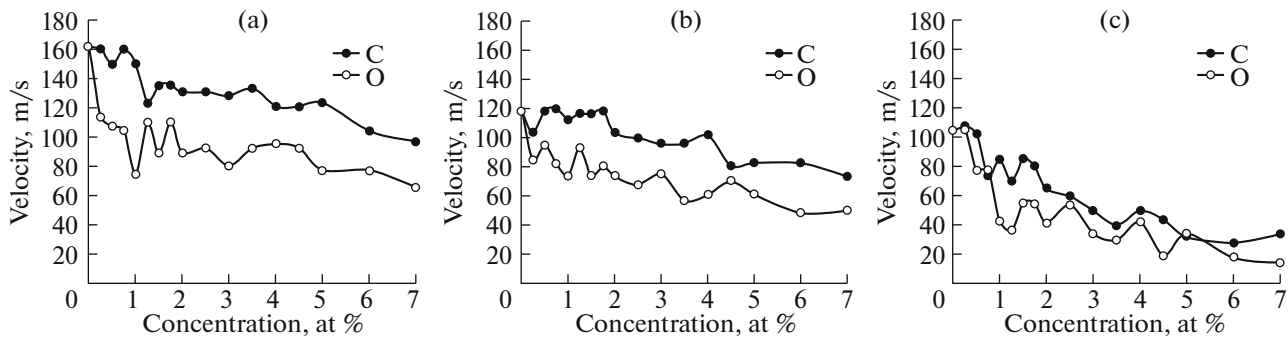


**Fig. 3.** Crystallization front motion velocity vs. the concentration of impurity carbon and oxygen atoms at the thermostat temperature 1200 K at the front orientation along planes (a) (100), (b) (110), and (c) (111).

The kinetic Wilson–Frenkel diffusion limited model describing the heterogeneous crystallization front kinetics is given by the relationship [1, 4, 6, 7]

$$v(T) = A \exp\left(-\frac{E}{kT}\right) \left[1 - \exp\left(-\frac{\Delta\mu}{kT}\right)\right], \quad (1)$$

where  $A$  is a pre-exponential factor,  $E$  is the activation energy of migration of atoms in liquid phase,  $k$  is the Boltzmann constant,  $T$  is temperature, and  $\Delta\mu$  is the difference of free energies of liquid and crystalline states.

It is evident, judging on Eq. (1), that the existence of impurity atoms influences  $E$  and  $\Delta\mu$ . The migration energy of atoms in the melt  $E$  will increase with the impurity concentration as a result of formation of comparative strong bonds between metal and impurity atoms and, as a result of these bonds, the deceleration of diffusion in the liquid metal; the value of  $\Delta\mu$  will decrease due to the distortion of the crystal lattice of the building crystal, as a result of the presence of the impurities. Both these factors decrease the crystallization velocity, as is seen from Eq. (1). A stronger coupling between a nickel atom and an impurity atom is characteristic of oxygen [15]; moreover, an oxygen atom in the nickel lattice leads to larger, as compared

to carbon atom, displacement of neighboring nickel atoms and the deformation of the crystal lattice surrounding the impurity atom [21]. Both these factors are the causes of the high influence of the oxygen impurity on the crystallization velocity as compared to carbon.

Figure 4 depicts the distributions of impurity carbon and oxygen atoms at concentration 7% in the computational cell with the (100) front orientation after the simulation of the crystallization for 75 ps at a temperature of 1500 K. As is seen in Fig. 4a, in the case of the quite high concentrations of carbon impurities, carbon atoms form aggregates, which are clusters consisting of several dozen of carbon atoms in the metal matrix. The crystallization front was decelerated on these clusters. During the crystallization in the presence of oxygen impurities clusters were not observed (Fig. 4b); however, the crystallization front deceleration was stronger as compared to the case of carbon impurities at the same concentrations

We observed similar behavior of the impurities, when studying their influence on the migration velocity of tilt-type boundaries with disorientation axes  $\langle 100 \rangle$  and  $\langle 111 \rangle$  in Ni, Ag, and Al [20]. The introduction of 5 at % impurities led to a significant decrease in

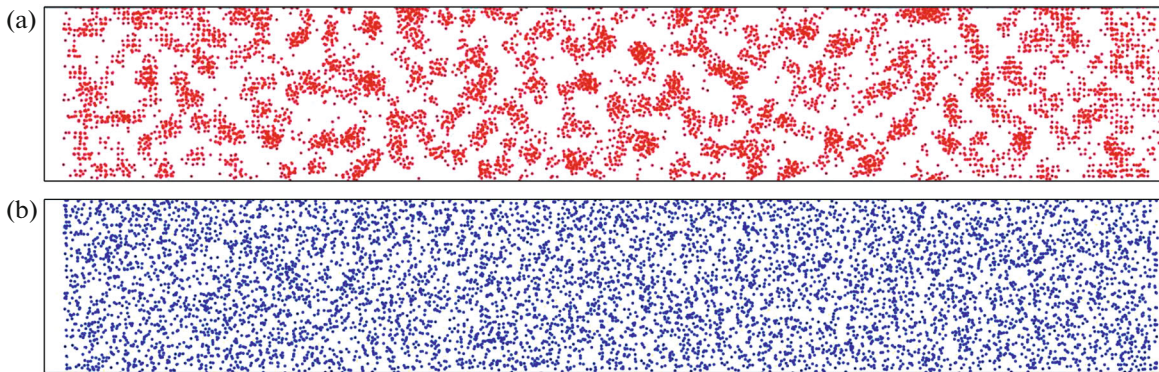


**Fig. 4.** Distribution of (a) carbon and (b) oxygen impurity atoms at the concentration 7 at % in the computational cell at front orientation (100) at a temperature of 1500 K.

the migration velocity of grain boundaries almost by one order of magnitude. The carbon atoms also formed clusters which effectively decelerated the boundary migration pinning on it. The impurity oxygen atoms did not form clusters, as in our experiment, but they also decelerated the boundary migration due to high binding energy with grain boundary due to the dilatation effect.

From Figs. 2, 3, it is seen that the crystallization front orientation influences the crystallization velocity: the crystallization velocity was higher at orientation (100) and lower at orientation (111). As we have mentioned in Introduction, this result was also obtained in [5, 9–12], where the studies were carried out by the molecular-dynamics method. The crystallization velocity anisotropy is likely determined, to a higher degree, by the dependence of  $\Delta\mu$  on the front orientation. This quantity is usually determined as the difference of the free energies of an atom in the melt and in the crystal lattice. However, we assume that, in this case, the higher significance has the difference of the free energies of an atom near the boundary in the liquid phase and a growing crystal “embedded” into the boundary, rather than the difference of energies in the crystal and liquid bulks. If  $\Delta\mu$  is defined from this point of view, it is likely to begin to be dependent on the crystallization front orientation with respect to the growing crystal. To confirm this fact, we specially found the values of the potential energy of a Ni adatom on the (111) and (100) surfaces of a nickel crystal (−2.67 and −2.85 eV, respectively). That is, as may be expected, the addition of an atom from the melt to the (100) surface is energetically more preferably than that to the (111) surface. In the addition to our calculations, we can call attention to the difference of the activation energies of migration of adatoms over surfaces (100) and (111), which are 0.63 and 0.33 eV, respectively, according to the results of the computer simulation in [22].

One further interesting peculiarity is the nontrivial temperature dependence of the crystallization front

velocity. As can be seen in Fig. 3, the velocities at 1200 K are higher than at 1500 K. In [8], we already singly considered the influence of temperature on the heterogeneous crystallization velocity. As the temperature decreases, the crystallization front motion velocity first increases, achieving the maximum at approximately  $0.7T_m$  (i.e., exactly at 1200 K), and then it smoothly decreases. The decrease in the crystallization front velocity with further overcooling is explained, according to the Wilson–Frenkel diffusion limited model, by the deceleration of the self-diffusion in the melt as the temperature decreases.

## CONCLUSIONS

The influence of carbon and oxygen impurities on the crystallization front motion velocity in nickel has been studied by the molecular-dynamics simulation. It was found that the addition of impurity atoms substantially decreases the crystallization front motion velocity, and oxygen atoms decelerate the crystallization front stronger than carbon atoms do. The crystallization deceleration mechanism with the impurity atoms is related to two factors: the deceleration of the self-diffusion in the liquid metal due to the formation of comparative strong bonds between the metal atoms and the impurity atoms (this bond for oxygen is stronger than that for carbon atoms) and the crystal lattice distortion due to the dilatation effect around the impurity atoms in the growing crystal (this effect is also higher in the case of oxygen atoms).

In the case of quite high carbon impurity concentrations (several percent), the carbon atoms formed aggregates which are clusters of several tens of carbon atoms in the metal matrix. The crystallization front was halted on these aggregates. No such aggregates were observed during the crystallization in the presence of oxygen impurity.

The crystallization front orientation influences the crystallization velocity: it is higher at orientation (100) and lower at orientation (111). This anisotropy of the

crystallization front motion velocity is due to the difference between the free energies of the metal atom in the liquid phase and the metal atom “embedded” into the growing crystal boundary.

## REFERENCES

1. P. K. Galenko, V. Ankudinov, K. Reuther, M. Rettenmayr, A. Salhoumi, and E. V. Kharanzhevskiy, *Philos. Trans. R. Soc., Ser. A* **377**, 20180205 (2019).  
<https://doi.org/10.1098/rsta.2018.0205>
2. S. K. Jha, S. Karthika, and T. K. Radhakrishnan, *Resour.-Effic. Technol.* **3**, 94 (2017).  
<https://doi.org/10.1016/j.reffit.2017.01.002>
3. V. Y. Stetsenko, *Lit'ye Metall.* **69**, 48 (2013).
4. V. I. Mazhukin, A. V. Shapranov, V. E. Perezhigin, O. N. Koroleva, and A. V. Mazhukin, *Math. Models Comput. Simul.* **9**, 448 (2017).  
<https://doi.org/10.1134/S2070048217040081>
5. M. I. Mendeleev, F. Zhang, H. Song, Y. Sun, C. Z. Wang, and K. M. Ho, *J. Chem. Phys.* **148**, 214705 (2018).  
<https://doi.org/10.1063/1.5026922>
6. G. Sun, J. Xu, and P. Harrowell, *Nat. Mater.* **17**, 881 (2018).  
<https://doi.org/10.1038/s41563-018-0174-6>
7. W.-L. Chan, R. S. Averbach, D. G. Cahill, and Y. Ashkenazy, *Phys. Rev. Lett.* **102**, 095701 (2009).  
<https://doi.org/10.1103/PhysRevLett.102.095701>
8. G. M. Poletaev, I. V. Karakulova, and D. K. Podorova, *Fundam. Probl. Sovrem. Materialoved.* **18**, 297 (2021).  
<https://doi.org/10.25712/ASTU.1811-1416.2021.03.006>
9. H. Y. Zhang, F. Liu, Y. Yang, and D. Y. Sun, *Sci. Rep.* **7**, 10241 (2017).  
<https://doi.org/10.1038/s41598-017-10662-x>
10. M. I. Mendeleev, M. J. Rahman, J. J. Hoyt, and M. Asta, *Model. Simul. Mater. Sci. Eng.* **18**, 074002 (2010).  
<https://doi.org/10.1088/0965-0393/18/7/074002>
11. J. J. Hoyt, M. Asta, and A. Karma, *Interface Sci.* **10**, 181 (2002).  
<https://doi.org/10.1023/A:1015828330917>
12. D. Y. Sun, M. Asta, and J. J. Hoyt, *Phys. Rev. B* **69**, 024108 (2004).  
<https://doi.org/10.1103/PhysRevB.69.024108>
13. G. M. Poletaev and I. V. Zorya, *Tech. Phys. Lett.* **46**, 575 (2020).  
<https://doi.org/10.1134/S1063785020060231>
14. F. Cleri and V. Rosato, *Phys. Rev. B* **48**, 22 (1993).  
<https://doi.org/10.1103/PhysRevB.48.22>
15. G. M. Poletaev, I. V. Zorya, R. Y. Rakitin, and M. A. Iliina, *Mater. Phys. Mech.* **42**, 380 (2019).  
[https://doi.org/10.18720/MPM.4242019\\_2](https://doi.org/10.18720/MPM.4242019_2)
16. R. Yu. Rakitin, G. M. Poletaev, M. S. Aksenov, and M. D. Starostenkov, *Tech. Phys. Lett.* **31**, 650 (2005).  
<https://doi.org/10.1134/1.2035354>
17. C. Chen, F. Zhang, H. Xu, Z. Yang, and G. M. Poletaev, *J. Mater. Sci.* **57**, 1833 (2022).  
<https://doi.org/10.1007/s10853-021-06837-7>
18. G. M. Poletaev, *J. Exp. Theor. Phys.* **133**, 455 (2021).  
<https://doi.org/10.1134/S1063776121090041>
19. G. M. Poletaev and I. V. Zorya, *J. Exp. Theor. Phys.* **131**, 432 (2020).  
<https://doi.org/10.1134/S1063776120080038>
20. G. M. Poletaev, I. V. Zorya, R. Y. Rakitin, M. A. Iliina, and M. D. Starostenkov, *Lett. Mater.* **9**, 391 (2019).  
<https://doi.org/10.22226/2410-3535-2019-4-391-394>
21. I. V. Zorya, G. M. Poletaev, and M. D. Starostenkov, *Fundam. Probl. Sovrem. Materialoved.* **15**, 526 (2018).  
<https://doi.org/10.25712/ASTU.1811-1416.2018.04.012>
22. C. L. Liu, J. M. Cohen, J. B. Adams, and A. F. Voter, *Surf. Sci.* **253**, 334 (1991).  
[https://doi.org/10.1016/0039-6028\(91\)90604-Q](https://doi.org/10.1016/0039-6028(91)90604-Q)

*Translated by Yu. Ryzhkov*